Relieving the S_8 tension: Exploring the surface-type DBI model as a dark matter paradigm

Xingpao Suo[*]

Institute for Astronomy, School of Physics, Zhejiang University, Hangzhou 310027, China

Xi Kang[†]

Institute for Astronomy, School of Physics, Zhejiang University, Hangzhou 310027, China
and Purple Mountain Observatory, 10 Yuan Hua Road, Nanjing 210034, China

Huanyuan Shan[‡]

Shanghai Astronomical Observatory (SHAO), Nandan Road 80, Shanghai 200030, China

Recent observations from weak gravitational lensing (WL) surveys indicate a smoother Universe compared to the predictions of the cosmic microwave background (CMB). This inconsistency is commonly referred to as the σ_8 tension or S_8 tension, where σ_8 represents the present root-mean-square matter fluctuation averaged over a sphere of radius $8h^{-1}$ Mpc, and $S_8 \equiv \sigma_8\sqrt{\Omega_m/0.3}$. In this article, we investigate a kind of general Dirac-Born-Infeld (DBI) Lagrangian referred to as the *surface-type DBI* (sDBI) model. We find that up to the linear order, the constraints on the sDBI model with high-redshift probe (CMB) and low-redshift probes (WL and galaxy clustering, GC) yield $S_8 = 0.7448^{+0.031}_{-0.21}$ and $0.7426^{+0.054}_{-0.085}$, respectively. Remarkably, these values not only demonstrate self-consistency but also align with the values obtained from the majority of low-redshift probes. Furthermore, we present a discussion on exploring the nonlinear effects of this model, which holds the potential to address additional challenges associated with cold dark matter (CDM) on small scales.

I. INTRODUCTION

The ΛCDM model stands as the most widely accepted cosmological model, serving as the standard framework for big bang cosmology. While the ΛCDM model provides a straightforward and successful description that aligns with a wide range of observations, the advancement of theoretical and observational studies has brought to light certain inconsistencies. These disparities, whether arising from conflicts between different observations or discrepancies between theory and observations, have begun to challenge the ΛCDM model, indicating the necessity for new extended models or alternative physics [1]. Among the various challenges faced by the ΛCDM model, the issue of σ_8 or S_8 tension stands out as one of the most prominent [2]. It shows that the low-redshift probes such as weak gravitational lensing (WL) [3,4], galaxy clustering (GC) [5,6] as well as their combined analyses [7,8], indicate a smoother Universe than the prediction by cosmic microwave background (CMB) [9]. Quantitatively, the

structure growth parameter S_8 derived from low-redshift probes consistently shows a $2 - 3\sigma$ lower value compared to the value obtained from the CMB [1,3,8–16]. Recently, a joint cosmological analysis of cosmic shear + galaxy-galaxy lensing + GC yielded a constraint of $(\Omega_m, S_8) = (0.305^{+0.010}_{-0.015}, 0.766^{+0.020}_{-0.014})$ (see [8], hereafter referred as $K1K$-3×2 pt), where S_8 is low by $8.3 \pm 2.6\%$ compared to $(\Omega_m, S_8) = (0.3166 \pm 0.0084, 0.834 \pm 0.016)$ given by baseline of *Planck2018* [9].

Some new models has been proposed to solve or relieve S_8 tension, such as an additional scaling parameter on the CMB lensing amplitude [17,18], a dark energy and dark matter interaction model [19–21], and modified gravitation [22], most of which give a consistent result with both CMB and low-redshift probes.

In this article, we propose a novel dark matter model that provides an alternative framework to resolve the S_8 tension. Our model, referred to as the sDBI model, introduces an area functional form as the dark matter Lagrangian, representing a specific instance within the broader class of general DBI models. Our investigation showcases the efficacy of this model in alleviating the S_8 tension by attenuating the formation of structures at low redshifts

[*]xpsuo@zju.edu.cn
[†]kangxi@zju.edu.cn
[‡]hyshan@shao.ac.cn

while maintaining the accurate evolution of perturbations at high redshifts.

II. THE SURFACE-TYPE DBI AS A DARK MATTER MODEL

Here we consider the Lagrangian

$$\mathcal{L} \equiv \frac{R}{2\kappa} + \Lambda_I + \Lambda_{II}\sqrt{1 + \partial_\mu\phi\partial^\mu\phi} + \mathcal{L}_m \qquad (1)$$

and its corresponding action $S = \int d^4x\sqrt{-g}\mathcal{L}$, where $g \equiv \det(g_{\mu\nu})$ represents the determinant of the space-time metric $g_{\mu\nu}$ with signature $[-1, 1, 1, 1]$, R denotes the scalar curvature of Levi-Civita connection, $\kappa \equiv 8\pi G$ with gravitational constant G, Λ_I is the vacuum energy or equivalently cosmological constant, $\mathcal{L}_m$ is the Lagrangian of normal matter including radiation and baryon, and $\Lambda_{II}\sqrt{1 + \partial_\mu\phi\partial^\mu\phi}$ with a constant Λ_{II} and scalar field ϕ is the Lagrangian that we introduce to represent dark matter, which we refer to as the surface-type Dirac-Born-Infeld (sDBI) model. Note that the term *surface-type* comes from a mathematical standpoint. The term $\int d^4x\sqrt{-g}\sqrt{1 + \partial_\mu\phi\partial^\mu\phi}$ can be viewed as formal area functional, which is usually used to describe the area of a surface. Meanwhile, it is worth mentioning that the sDBI possesses strong physical motivation, see [23–27].

For the Lagrangian given in Eq. (1), applying the principle of least action gives the Einstein field equation:

$$R_{\mu\nu} - \frac{1}{2}Rg_{\mu\nu} = -\kappa\left(T_{\mu\nu}^{(\Lambda_I)} + T_{\mu\nu}^{(\Lambda_{II})} + T_{\mu\nu}^{(m)}\right), \qquad (2)$$

where $R_{\mu\nu}$ is the Ricci tensor, $T_{\mu\nu}^{(\Lambda_I)} = -\Lambda_I g_{\mu\nu}$ and

$$T_{\mu\nu}^{(\Lambda_{II})} = \Lambda_{II}\left(\frac{\partial_\mu\phi\partial_\nu\phi}{\sqrt{1 + \partial_\rho\phi\partial^\rho\phi}} - g_{\mu\nu}\sqrt{1 + \partial_\rho\phi\partial^\rho\phi}\right) \qquad (3)$$

represent the energy-stress tensor of dark energy and dark matter in this model, respectively. Now our focus turns to the sDBI field. According to Eq. (3), in the flat, homogeneous, and isotropic background of the Universe, sDBI field can be treated as a perfect fluid characterized by the equation of state (EoS, see Appendix A 1)

$$w = -\frac{\Lambda_{II}^2}{\rho^2}, \qquad (4)$$

where $w \equiv P/\rho$, P and ρ denoting the pressure and mass density of the sDBI field, respectively. The evolution of ρ and w regard to scale factor a can be derived as (see Appendix A 1)

$$\rho(a) = \Lambda_{II}a_d^3\sqrt{a_d^{-6} + a^{-6}} \equiv \rho_s\sqrt{a_d^{-6} + a^{-6}} \qquad (5)$$

and

$$w(a) = -\frac{1}{1 + \left(\frac{a_d}{a}\right)^6}, \qquad (6)$$

respectively. Here, the scale factor a is normalized to unity at the present time, and a_d is a free parameter that we call as decay parameter.

Moreover, considering a linear perturbation in the homogeneous Universe, the sound speed of the sDBI field can be given by (see Appendix A 2)

$$c_s^2 = c_a^2 = -w, \qquad (7)$$

where $c_s \equiv \delta P/\delta\rho$ and $c_a \equiv dP/d\rho$ are the effective and adiabatic sound speed, respectively. The EoS and sound speed provide sufficient information to complete the scalar linear evolution equations of Universe [28,29].
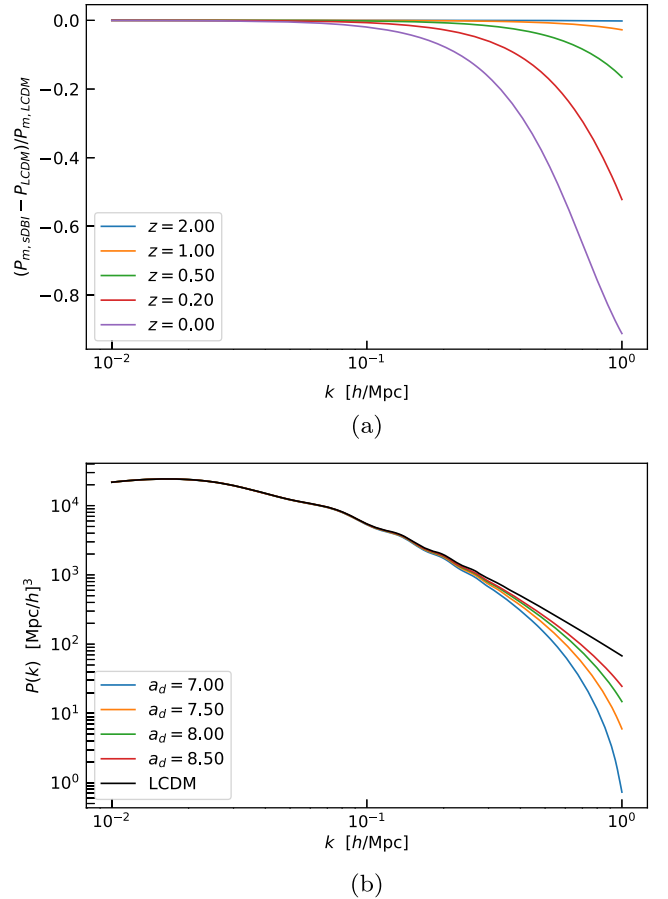

FIG. 1. (a) The suppression of sDBI on matter power spectrum for different redshifts, where $\Delta P_k \equiv P_k^{(\text{sDBI})} - P_k^{(\Lambda\text{CDM})}$ with a_d set to 3.8. (b) The matter power spectrum at redshift $z = 0$ for different a_ds. When $a_d \to \infty$, the power spectrum asymptotically approaches the ΛCDM model (black line). In both figures, the fixed parameters are taken from the best fit of the sDBI model in Table II.

The dark matter with the above form EoS and sound speed has such properties that during the early stages ($a \ll a_d$), it behaves similarly to the pressure-less standard cold dark matter, but at the late stages (a close to a_d), it exhibits a certain sound speed and pressure, which leads to the smoothing out the structures that formed during the early stages [30–33]. This may provide an explanation for the smoother Universe at low-redshift. In Fig. 1(a), we illustrate the difference between the linear matter spectra of the sDBI and the ΛCDM model. It is evident that the sDBI suppresses the power spectra in the late-stage Universe. The value of the decay parameter will greatly influence this process. Figure 1(b) shows the power spectra for different a_ds at $z = 0$. As a_d tends toward infinity, the sDBI model will degenerate to ΛCDM. Some similar late-time schemes have also been proposed [13,34], offering viable solutions to the S_8 tension. The sDBI may serve as a theoretical framework for these late-time schemes.

Note that in the nonlinear region, we strictly need to consider Eq. (2) and the evolution equation for ϕ

$$\left(\frac{1}{2}\partial_\mu \log(-g) + \partial_\mu\right) \frac{\partial^\mu \phi}{\sqrt{1 + \partial_\nu \phi \partial^\nu \phi}} = 0, \qquad (8)$$

which represents a general minimal surface equation. However, in this work, we focus solely on the scalar linear perturbation, as it dominates the evolution of dark matter, especially on large scales and during the early stages of our Universe.

III. CONSTRAINTS BY THE OBSERVATIONS

To demonstrate that the sDBI model can alleviate the S_8 tension, we perform a series of constraints using different observational datasets. We begin with the baseline of *Planck2018*, which combines the *TT*, *TE*, *EE*, and low-*E* angular power spectra of the CMB to constrain the cosmological parameters [9]. This base line analysis is advantageous as it avoids model-dependent nonlinear effects that may introduce uncertainties [35,36]. For the low-redshift probes, we employ the WL shear catalog from KiDS1000 [3,37] and the GC data from SDSS-III BOSS [38]. In these analyses, we treat the high-redshift probe (CMB) and low-redshift probes (WL and GC) separately, rather than combining them. If the two datasets can give a consistent result, it will provide stronger evidence in support of the model's validity. In addition, we simultaneously constrain the ΛCDM model as a control group for comparison purposes.

Utilizing the EoS (4) and sound speed (7), we have adapted the background and perturbation equations, as implemented in the Boltzmann code CLASS-v3.2.0 [39,40], to calculate the linear evolution of the Universe. And a public Markov Chain Monte Carlo (MCMC) sampler

TABLE I. The symbols and prior of cosmological parameters, where the infinity symbols $\pm\infty$ mean that we do not limit the upper/lower bound of the corresponding parameter.

Parameter	Symbol	Prior
Baryon density	ω_b	$[-\infty, \infty]$
Dark matter density	Ω_s	$[0, \infty]$
Inverse of decay parameter	a_d^{-1}	$(0, \infty]$
Reduced Hubble constant	h	$[-\infty, \infty]$
Scalar fluctuation amplitude	A_s	$[-\infty, \infty]$
Scalar spectral index	n_s	$[-\infty, \infty]$
Reionization optical depth	τ_{reio}	$[0.004, \infty]$

Monte Python-v3.2 [41–43] was used. We perform all the MCMC samplings for our constraints using the Metropolis-Hastings algorithm implemented in Monte Python-v3.2.

To constrain this model with the *Planck2018* baseline, we adopt a flat prior on certain nuisance parameters in the *Planck* likelihood (Plik) [44], as well as on the cosmological parameters $\{\omega_b, \Omega_s, h, A_s, n_s, \tau_{\mathrm{reio}}, a_d\}$, where

$$\Omega_s \equiv \frac{\rho_s}{\rho_{cr}} \equiv \frac{8\pi G}{3H_0^2} \rho_s \qquad (9)$$

is the reduced dark matter density in our model. The names and priors of the base cosmological parameters are provided in Table I. For comparison, we have also conducted a parallel ΛCDM constraint. Note that in all the analyses, we assume a flat universe with zero spatial curvature ($\Omega_K = 0$). Additionally, our neutrino model follows the same configuration as *Planck2018*, consisting of two massless species and one massive species with a mass of 0.06 eV.

The posterior distributions obtained with *Planck2018* baseline are presented in Table II. The Markov chain employed in the analysis satisfies the Gelman-Rubin convergence criterion with $R - 1 \approx 10^{-3}$, indicating robust convergence. Furthermore, our constraints on the ΛCDM model are consistent with the results reported by the *Planck2018* collaboration [9], validating the accuracy of this analysis.

The results reveal slight differences in common cosmological parameters between the sDBI and ΛCDM. However, significant discrepancies have been observed in the structure growth parameter S_8. The sDBI model yields values of $(\Omega_m, S_8) = (0.3199^{+0.0095}_{-0.0095}, 0.7448^{+0.031}_{-0.21})$, which agree with the results from *K1K*-3×2 pt within 1σ and clearly deviate from the result given by *Planck2018*.

Note there is a relatively larger credible interval for both S_8 or σ_8. To further understand it, we fix the cosmological parameters except a_d to the best fit in Table II, then calculate S_8 and χ_ν^2 for different a_ds. Here the reduced chi-square χ_ν^2 is defined as chi-squared divided by the degrees of freedom

TABLE II. The best-fit values, mean values, 68% credible intervals and χ^2 for the sDBI and ΛCDM models from *Plank* CMB power spectrum. The first 8 parameters consist of the base parameters, which include 5 common parameters and 3 peculiar parameters specific to each model (Ω_s and a_d for sDBI, and Ω_{cdm} for ΛCDM). The last 4 parameters are derived quantities, where Ω_{vac} is defined as Ω_Λ and Ω_{Λ_I} in the ΛCDM and sDBI models, respectively. Additionally, we use the notation $\Omega_m \equiv 1 - \Omega_{vac}$ for both models. This term represents the sum of the density parameters of all components in the Universe, excluding the contribution from dark energy.

Parameters	sDBI		ΛCDM	
	Best fit	mean$^{+\sigma}_{-\sigma}$	Best fit	mean$^{+\sigma}_{-\sigma}$
Ω_s	0.2687	$0.2688^{+0.0087}_{-0.0089}$		
a_d^{-1}	0.1476	$0.1190^{+0.080}_{-0.078}$		
Ω_{cdm}			0.2686	$0.2678^{+0.0086}_{-0.0075}$
$100\omega_b$	2.233	$2.233^{+0.014}_{-0.015}$	2.224	$2.233^{+0.015}_{-0.015}$
h	0.6709	$0.6706^{+0.0068}_{-0.0067}$	0.6704	$0.6713^{+0.0060}_{-0.0066}$
$10^9 A_s$	2.089	$2.110^{+0.037}_{-0.031}$	2.089	$2.107^{+0.033}_{-0.033}$
n_s	0.9628	$0.9619^{+0.0046}_{-0.0044}$	0.9630	$0.9628^{+0.0042}_{-0.0040}$
τ_{reio}	0.05017	$0.05524^{+0.0079}_{-0.0069}$	0.05101	$0.05472^{+0.0079}_{-0.0072}$
Ω_{vac}	0.6802	$0.6800^{+0.0095}_{-0.0095}$	0.6804	$0.6811^{+0.0080}_{-0.0095}$
S_8	0.7751	$0.7448^{+0.031}_{-0.21}$	0.8364	$0.8384^{+0.017}_{-0.016}$
σ_8	0.7508	$0.7214^{+0.019}_{-0.21}$	0.8105	$0.8133^{+0.0083}_{-0.0077}$
Ω_m	0.3197	$0.3199^{+0.0095}_{-0.0095}$	0.3195	$0.3188^{+0.0095}_{-0.0080}$
χ^2	2749.20		2749.38	

$$\chi_\nu^2 \equiv \frac{1}{N-n}\chi^2 \equiv \frac{1}{N-n}\sum_{i=1}^{N}\frac{(O_i - C_i)^2}{\sigma_i^2} \quad (10)$$

with O_i and σ_i the ith observed mean value and measure error, respectively, C_i the corresponding prediction, N the number of observed values, n the number of fitted parameters.

The results are shown in Fig. 2, where $\Delta\chi_\nu^2 \equiv \chi_\nu^2 - \chi_{\nu,b}^2$ with $\chi_{\nu,b}^2 \approx 1.038422$ the chi-square for the best fit. Visibly, the fitting is almost as good as the best fit if $a_d \gtrsim 6$, where, however, the S_8 can still vary from about 6.5 to about 0.8. In other words, the sDBI model can decrease the value of S_8 without influence CMB power spectra. In addition, it is worth noting that based on this mechanism, the sDBI model does not aggravate the Hubble tension.

After constraining the models using *Planck2018* CMB power spectra, we proceed to perform a combined constraint by incorporating low-redshift probes, specifically WL and GC. Once again, we carry out parallel constraints for both the sDBI and ΛCDM models. Our approach to the correlation function involves mitigating nonlinear
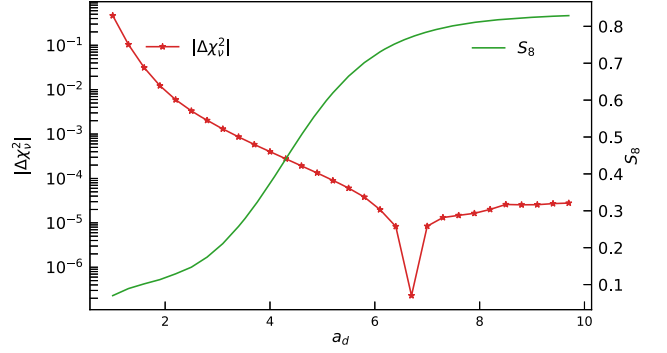

FIG. 2. The $|\Delta\chi_\nu^2|$ (red) and S_8 (green) regard to the decay parameter a_d, where $\Delta\chi_\nu^2 \equiv \chi_\nu^2 - \chi_{\nu,b}^2$ with $\chi_{\nu,b}^2 \approx 1.038422$ the chi-square for the best fit. The drop near $a_d = 6.5$ is due to its proximity to the best fit.

effects due to their unavailability in our model. For WL, we employ the correlation function $\xi_+(\theta)$ and implement a truncation to the small-scale region ($\theta < 10$) using the KiDS cosmology analysis pipeline kcap [45,46]. The truncation is achieved through the following steps: First, we separately calculate the correlation function data vectors with and without the nonlinear effect with kcap, and label them by ξ_+^{NL} and ξ_+^L, respectively. Subsequently, we calculate the relative distance between the output data vectors, denoted as d_c and defined by $\|\xi_+^{NL} - \xi_+^L\|/\|\xi_+^{NL}\|$ with $\|\cdot\| \equiv \sqrt{\langle\cdot,\cdot\rangle}$. If d_c exceeds a threshold of 10^{-2}, we utilize kcap to remove some small-scale data points. This process is iteratively repeated until d_c falls below 10^{-2}. Note that we have excluded the correlation function ξ_- from our analysis as the nonlinear effects on ξ_- are difficult to mitigate.

For GC, our analysis specifically focuses on the measurements of the baryon acoustic oscillations (BAO) while excluding the consideration of redshift-space distortions. Due to the strict elimination of the nonlinear effect, the constraint on the five common base parameters becomes weaker. Hence, for both the sDBI and ΛCDM models, we fix these parameters according to their respective best-fit values in Table II.

The ΛCDM model constraint yields $(\Omega_m, S_8) = (0.299^{+0.011}_{-0.0105}, 0.770^{+0.0371}_{-0.035})$, which is consistent with the results obtained from *K1K*-3 × 2 pt. However, it is evident that S_8 remains lower compared to the *Planck2018* baseline. As depicted in Fig. 3(a), the tension between low-redshift probes and the CMB persists.

In contrast, for the sDBI model, the tension in S_8 is absent. As illustrated in Fig. 3(b), the constraint provides $(\Omega_m, S_8) = (0.306^{+0.014}_{-0.014}, 0.7426^{+0.054}_{-0.085})$, which is consistent within 1σ compared to our constraint using the *Planck2018* baseline.
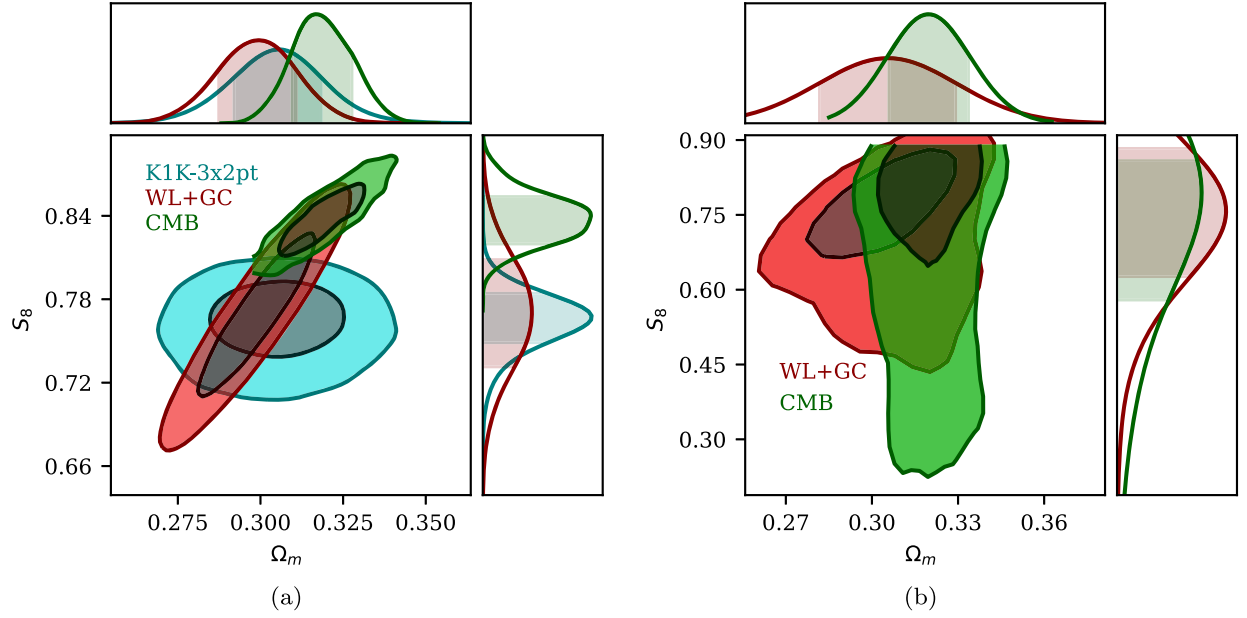
FIG. 3.   The posterior distributions given by high-redshift probe (CMB) and low-redshift probes (WL + GC). For low-redshift probes, the five common parameters are fixed to the values given in Table II for respective models. (a) The posterior distributions of Ω_m and S_8 for ΛCDM model, where we also plot the result from $K1K$-3 × 2 pt for comparison. Note that even cut off the nonlinear effect, our low-redshift constraint is consistent with $K1K$-3 × 2 pt, and the tension of S_8 still exists. (b) Same as (a) but for the sDBI model. No tension exists.

IV. CONCLUSION AND DISCUSSION

In this article, we propose a so-called surface-type Dirac-Born-Infeld (sDBI) field as a dark matter candidate to relieve the S_8 tension. We have conducted a parallel investigation of the background and linear perturbation evolution for both the sDBI and standard ΛCDM models. The MCMC analysis with the data from early Universe (CMB) and late Universe (WL) reveals that the S_8 tension persists in the ΛCDM model even when considering only linear perturbations. This suggests that modifying the nonlinear model such as HALOFIT [35] or HMCode [36], is unlikely to resolve the tension effectively. On the other hand, the sDBI model, within the scope of the datasets we have considered, successfully alleviates the S_8 tension.

To obtain more accurate constraints on the parameter a_d, it is necessary to consider nonlinear effects, which can be studied by N-body simulations. In the nonrelativistic approximation, for the fluid described by Eq. (4), we can introduce an effective potential (see Appendix A 3)

$$h \equiv - \int_\rho^\infty \frac{dP(\rho')}{\rho'} = -\frac{1}{2}\frac{\Lambda_{II}^2}{\rho^2} \qquad (11)$$

to substitute the effect of pressure. Using an effective potential to describe the sDBI has the advantage that it can be easily incorporated into N-body simulation codes.

The potential described in Eq. (11) acts as a contrary effect from gravity, and the gradient of the potential

increases in conjunction with the decrease in energy density ρ over time. The increasing external force can partially disrupt the structures that formed in the early universe, potentially leading to the formation of galaxies with a lack of dark matter [47,48]. Furthermore, the external force may completely destroy certain dwarf galaxies [49]. We also anticipate a reduction in redshift-space distortion over time, as the relative motion between dark matter halos decelerates. The $S_8(z)$ test could serve as a robust assessment for this model, as the external potential is expected to significantly diminish the fluctuation amplitude of matter in the later stages. Meanwhile, there is a double coincidence problem inherent in a_d and Ω_{II}. In order to address this issue, a more fundamental theory will be required in the future to provide a resolution. Given the intricacy of these topics, we defer their exploration to future work.

APPENDIX: THE EVOLUTION AND FLUID EQUIVALENCE OF sDBI FIELD

1. The background evolution

For the curvature-free, homogeneous, and isotropic background of the Universe, the spacetime is described by the flat Friedmann-Lematre-Robertson-Walker (FLRW) metric

$$ds^2 = a^2(\tau)(-d\tau^2 + \delta_{ij}dx^i dx^j), \tag{A1}$$

where a is the scale factor, $\tau \equiv \int dt/a$ with cosmic time t is conformal time, (x^1, x^2, x^3) are the coordinates of space, δ_{ij} is Kronecker symbol. In such a Universe, the background evolution of the sDBI field is also solely dependent on time. Consequently, the energy-stress tensor (3) can be simplified as follows:

$$T_{00} = g_{00}\Lambda_{II}\frac{1}{\sqrt{1 - \phi'^2/a^2}} \equiv g_{00}\rho \tag{A2}$$

$$T_{ii} = -g_{ii}\Lambda_{II}\sqrt{1 - \phi'^2/a^2} \equiv g_{ii}P \tag{A3}$$

$$T_{ij} = T_{0i} = 0 \tag{A4}$$

where ρ and P are the energy density and pressure of the sDBI field, respectively, $i, j = 1, 2, 3$ with $i \neq j$, $g_{\mu\nu}$ is the metric tensor, $'$ denotes a derivative with respect to conformal time. Indeed, in this scenario, it follows that $P\rho = -\Lambda_{II}^2$, so sDBI field is equivalent to an ideal fluid with the EoS

$$w \equiv \frac{P}{\rho} = -\frac{\Lambda_{II}^2}{\rho^2}. \tag{A5}$$

By utilizing the Einstein field equation (2), one can derive the conservation law

$$T^\mu_{\nu;\mu} = G^\mu_{\nu;\mu} = 0. \tag{A6}$$

For the background of the Universe, Eq. (A6) can be simplified to

$$\rho' + 3\mathcal{H}(\rho + P) = 0 \tag{A7}$$

where $\mathcal{H} \equiv a'/a$ is the conformal Hubble parameter. One can change the independent variable in Eq. (A7) from time t to scale factor a

$$\frac{d\rho}{d\log a} + 3(\rho + P) = 0. \tag{A8}$$

Combining Eqs. (A5) and (A8) one gets the evolution of the energy density regard to the scale factor

$$\rho(a) = \Lambda_{II}a_d^3\sqrt{a_d^{-6} + a^{-6}} \equiv \rho_s\sqrt{a_d^{-6} + a^{-6}} \tag{A9}$$

and

$$w(a) = -\frac{1}{1 + \left(\frac{a_d}{a}\right)^6}, \tag{A10}$$

where the integration constant a_d is introduced, which we refer to as the decay parameter.

2. The linear perturbation evolution

When considering linear perturbations on the background metric in Eq. (A1) and neglecting vector and tensor perturbations while adopting the Newtonian gauge, one can express the perturbed metric as

$$ds^2 = a^2(\tau)\big(-(1 + 2\Psi)d\tau^2 + (1 + 2\Phi)\delta_{ij}dx^i dx^j\big), \tag{A11}$$

where Ψ and Φ are two spatial scalars referred to as Newtonian and curvature potential, respectively. By substituting Eq. (A11) into the Einstein equation (2) and considering only terms up to linear order, we can obtain the scalar perturbation equations for the sDBI field

$$\delta' = -3(c_s^2 - w)\mathcal{H}\delta - (1 + w)(\theta + 3\Phi')$$

$$\theta' = -(1 - 3c_s^2)\mathcal{H}\theta - \nabla^2\left(\frac{c_s^2}{1 + w}\delta + \Psi\right) \tag{A12}$$

where $\delta \equiv (\rho - \bar{\rho})/\bar{\rho}$ is the density contrast with the density ρ and averaged density $\bar{\rho}$, $\theta \equiv \nabla \cdot \mathbf{u}$ is the velocity divergence with $\mathbf{u}$ the velocity of the fluid elementary, $c_s^2 \equiv \delta P/\delta\rho$ with the pressure perturbation δP and density perturbation $\delta\rho$ is the effective sound speed.

In realistic calculations, the gravitational potentials Ψ and Φ are determined by considering contributions from all components of the Universe. These contributions can be obtained through linearized Einstein equations. The conformal Hubble parameter $\mathcal{H}$ is obtained during the calculation of background evolution. Consequently, the effective sound speed c_s^2 becomes the only degree of freedom that requires specification.

To obtain the effective sound speed c_s^2 in the sDBI model, one considers a perturbation $\delta\phi$ on the background sDBI field ϕ. The perturbed energy-stress caused by $\delta\phi$ is given by

$$\delta T_\nu^\mu = \frac{\partial T_\nu^\mu}{\partial \phi}\delta\phi + \frac{\partial T_\nu^\mu}{\partial(\partial_\alpha\phi)}\delta(\partial_\alpha\phi) + \frac{\partial T_\nu^\mu}{\partial g_{\alpha\beta}}\delta g_{\alpha\beta}, \quad \text{(A13)}$$

where T_ν^μ is given by Eqs. (A2)–(A4). The meticulous but straightforward calculation gives the linear order perturbation

$$\delta\rho = -\delta T_0^0 = \frac{\Lambda_{II}}{(1-\phi'^2/a^2)^{3/2}a^2}\left(\frac{1}{2}\phi'^2\delta g^{00} + \phi'\delta\phi'\right) \quad \text{(A14)}$$

$$\delta P = \delta T_i^i = \frac{\Lambda_{II}}{(1-\phi'^2/a^2)^{1/2}a^2}\left(\frac{1}{2}\phi'^2\delta g^{00} + \phi'\delta\phi'\right), \quad \text{(A15)}$$

which gives

$$c_s^2 \equiv \frac{\delta P}{\delta\rho} = 1 - \frac{\phi'^2}{a^2} = -w. \quad \text{(A16)}$$

Note that the adiabatic sound speed of the sDBI field is

$$c_a^2 \equiv \frac{dP}{d\rho} = \frac{\Lambda_{II}^2}{\rho^2} = -w. \quad \text{(A17)}$$

It is evident that $c_s^2 = c_a^2$, and this relationship is not coincidental. The equation of state (EoS) given by Eq. (A5) demonstrates that the sDBI field can be regarded as a barotropic fluid, where the pressure P solely depends on the mass density ρ. In the case of a barotropic fluid, the effective sound speed is equal to the adiabatic sound speed.

3. The nonrelativistic fluid equivalence

Assuming that Newton's laws still apply to the sDBI fluid, the momentum equation can be expressed as

$$\frac{D\mathbf{u}}{Dt} = -\frac{\nabla P}{\rho} - \nabla\Psi, \quad \text{(A18)}$$

where $\mathbf{u}$ is the velocity of the fluid elementary, P and ρ are the pressure and mass density of the fluid, respectively, Ψ is the Newtonian gravitational potential, $D/Dt \equiv \partial/\partial t + \mathbf{u} \cdot \nabla$ is the material derivative. Introducing an effective potential h, one can rewrite Eq. (A18) as

$$\frac{D\mathbf{u}}{Dt} = -\nabla(h + \Psi), \quad \text{(A19)}$$

where h is defined by

$$h \equiv -\int_\rho^\infty \frac{dP(\rho')}{\rho'} = -\frac{1}{2}\frac{\Lambda_{II}^2}{\rho^2}. \quad \text{(A20)}$$

In the early stage of the Universe, $\rho \gg \Lambda_{II}$, thus $|h| \ll 1$ and the evolution is dominated by Ψ. However, in the late stage of the Universe, the role of the perturbation h gradually becomes more significant. In regions with higher matter density, the gravitational potential tends to have a larger value. This behavior is contrary to gravity, where regions with higher matter density typically exhibit a smaller gravitational potential.

[1] E. Abdalla *et al.*, J. High Energy Astrophys. **34**, 49 (2022).
[2] E. Di Valentino *et al.*, Astropart. Phys. **131**, 102604 (2021).
[3] Marika Asgari *et al.*, Astron. Astrophys. **645**, A104 (2021).
[4] T. M. C. Abbott *et al.* (DES Collaboration), Phys. Rev. D **105**, 023520 (2022).
[5] Laura Salvati, Marian Douspis, and Nabila Aghanim, Astron. Astrophys. **614**, A13 (2018).
[6] M. M. Ivanov, M. Simonovi, and M. Zaldarriaga, J. Cosmol. Astropart. Phys. 05 (2020) 042.
[7] P.-S. Corasaniti, M. Sereno, and S. Ettori, Astrophys. J. **911**, 82 (2021).
[8] Catherine Heymans *et al.*, Astron. Astrophys. **646**, A140 (2021).
[9] Planck Collaboration, Astron. Astrophys. **641**, A6 (2020).
[10] M. A. Troxel *et al.* (Dark Energy Survey Collaboration), Phys. Rev. D **98**, 043528 (2018).
[11] C. Hikage *et al.*, Publ. Astron. Soc. Jpn. **71**, 43 (2019).
[12] Angus H. Wright, Hendrik Hildebrandt, Jan Luca van den Busch, Catherine Heymans, Benjamin Joachimi, Arun Kannawadi, and Konrad Kuijken, Astron. Astrophys. **640**, L14 (2020).
[13] V. Poulin, J. L. Bernal, E. Kovetz, and M. Kamionkowski, Phys. Rev. D **107**, 123538 (2023).
[14] A. Amon *et al.* (DES Collaboration), Phys. Rev. D **105**, 023514 (2022).
[15] X. Li *et al.*, arXiv:2304.00702.
[16] R. C. Nunes and S. Vagnozzi, Mon. Not. R. Astron. Soc. **505**, 5427 (2021).
[17] E. Di Valentino and S. Bridle, Symmetry **10**, 585 (2018).
[18] E. Di Valentino, A. Melchiorri, and J. Silk, Phys. Rev. D **92**, 121302(R) (2015).
[19] E. Di Valentino, A. Melchiorri, O. Mena, and S. Vagnozzi, Phys. Dark Universe **30**, 100666 (2020).
[20] M. Lucca, Phys. Dark Universe **34**, 100899 (2021).
[21] E. Di Valentino, A. Melchiorri, O. Mena, and S. Vagnozzi, Phys. Rev. D **101**, 063502 (2020).
[22] Planck Collaboration *et al.*, Astron. Astrophys. **594**, A14 (2016).
[23] M. Alishahiha, E. Silverstein, and D. Tong, Phys. Rev. D **70**, 123505 (2004).
[24] L. P. Chimento, R. Lazkoz, and I. Sendra, Gen. Relativ. Gravit. **42**, 1189,1209 (2010).
[25] M. Bordemann and J. Hoppe, Phys. Lett. B **317**, 315 (1993).

[26] M. Bordemann and J. Hoppe, Phys. Lett. B **325**, 359 (1994).
[27] N. Ogawa, Phys. Rev. D **62**, 085023 (2000).
[28] W. Hu, Astrophys. J. **506**, 485 (1998).
[29] W. Hu, ICTP Lect. Notes Ser. **14**, 145 (2003), https://arxiv.org/abs/astro-ph/0402060.
[30] V. Gorini, A. Kamenshchik, and U. Moschella, Phys. Rev. D **67**, 063509 (2003).
[31] N. Bili, G. Tupper, and R. Viollier, Phys. Lett. B **535**, 17 (2002).
[32] F. Salahedin, R. Pazhouhesh, and M. Malekjani, Eur. Phys. J. Plus **135** (2020).
[33] S. A. Adil, Ö. Akarsu, M. Malekjani, E. Ó. Colgáin, S. Pourojaghi, A. A. Sen, and M. M. Sheikh-Jabbari, arXiv:2303.06928.
[34] M.-X. Lin, B. Jain, M. Raveri, E. J. Baxter, C. Chang, M. Gatti, S. Lee, and J. Muir, arXiv:2308.16183.
[35] R. E. Smith, J. A. Peacock, A. Jenkins, S. D. M. White, C. S. Frenk, F. R. Pearce, P. A. Thomas, G. Efstathiou, and H. M. P. Couchman, Mon. Not. R. Astron. Soc. **341**, 1311 (2003).
[36] A. J. Mead, C. Heymans, L. Lombriser, J. A. Peacock, O. I. Steele, and H. A. Winther, Mon. Not. R. Astron. Soc. **459**, 1468 (2016).

[37] K. Kuijken et al., Astron. Astrophys. **625**, A2 (2019).
[38] S. Alam et al., Mon. Not. R. Astron. Soc. **470**, 2617 (2017).
[39] D. Blas, J. Lesgourgues, and T. Tram, J. Cosmol. Astropart. Phys. 07 (2011) 034.
[40] https://lesgourg.github.io/class_public/class.html.
[41] T. Brinckmann and J. Lesgourgues, Phys. Dark Universe **24**, 100260 (2019).
[42] B. Audren, J. Lesgourgues, K. Benabed, and S. Prunet, J. Cosmol. Astropart. Phys. 02 (2013) 001.
[43] https://baudren.github.io/montepython.html.
[44] Planck Collaboration, Astron. Astrophys. **641**, A5 (2020).
[45] B. Joachimi et al., Astron. Astrophys. **646**, A129 (2021).
[46] J. Zuntz, M. Paterno, E. Jennings, D. Rudd, A. Manzotti, S. Dodelson, S. Bridle, S. Sehrish, and J. Kowalkowski, Astron. Comput. **12**, 45 (2015).
[47] P. van Dokkum et al., Nature (London) **555**, 629 (2018).
[48] G. Ogiya, F. C. van den Bosch, A. Burkert, and X. Kang, Astrophys. J. Lett. **940**, L46 (2022).
[49] H. Kase, J. Makino, and Y. Funato, Publ. Astron. Soc. Jpn. **59**, 1071 (2007).